Influence of Knudsen and Mach numbers on Kelvin-Helmholtz instability

Vishnu Mohan [*] and A Sameen [†]
Department of Aerospace Engineering, Indian Institute of Technology Madras, Chennai 600036, India

Balaji Srinivasan [‡]
Department of Mechanical Engineering, Indian Institute of Technology Madras, Chennai 600036, India

Sharath S. Girimaji [§]
Department of Ocean Engineering, Texas A&M University, College Station, Texas 77843, USA

(Received 31 December 2020; accepted 26 April 2021; published 14 May 2021; corrected 24 May 2021)

The combined influence of rarefaction and compressibility on classical Kelvin-Helmholtz instability is investigated with numerical simulations employing the unified gas kinetic scheme. Five different regimes in the Reynolds-Mach-Knudsen number parameter space are identified. The flow features in various Mach and Knudsen number regimes are examined. Stabilizing action of compressibility leads to suppression of perturbation kinetic energy and vorticity and/or momentum thickness. The suppression due to rarefaction exhibits a different behavior. At high enough Knudsen numbers, even as the perturbation kinetic energy is suppressed, the vorticity and/or momentum thickness grows. The flow physics underlying the contrasting mechanisms of compressibility and rarefaction is highlighted.

DOI: 10.1103/PhysRevE.103.053104

I. INTRODUCTION

Mixing layers fall in the category of free-shear flows, which include jets and wakes. These flows are susceptible to the Kelvin-Helmholtz (KH) instability due to inflection points present in the velocity profile. In the classical instability, the shear layer rolls up into vortices or billows about the inflection line entraining fluid from the freestream. In this paper, we examine the effect of rarefaction and compressibility on the onset of KH instability. Such a study is of practical value in understanding the rarefied jet plumes of satellite thrusters, slipstreams formed behind a Mach stem, and many other engineering and astrophysical flows. At the low Mach number limit, the effects of rarefaction can provide insight into mixing in micromechanical devices.

Based on the parallel-flow Orr-Sommerfeld equation, mixing layers are shown to be unconditionally unstable [1], leading to the inference that the critical Reynolds number (Re_{cr}) is zero for the onset of the instability. Villermaux [2] accounts for the diffusive growth of the base flow in the Orr-Sommerfeld equation, and provides a modification to the marginal stability curve of [1]. Inclusion of nonparallel effects [3] for a spatially developing laminar incompressible mixing layer base flow further increases the Re_{cr} to approximately 30. Convective Mach number [4], defined as $M_c = (U_1 - U_2)/(c_1 + c_2)$, where U_1 and U_2 are velocities of two streams with respective sound velocities c_1 and c_2, quantifies the compressibility effects in high-speed mixing layers. Lessen *et al.* [5] show that compressibility enhances the stability of mixing layers and that oblique waves are more unstable than streamwise waves at high convective Mach numbers. Sandham and Reynolds [6] show using linear stability analysis of inviscid compressible mixing layers that for $M_c > 0.6$, the disturbances became three dimensional. Numerical simulations of Navier-Stokes equation show that at higher M_c, the vortical structures are more oblique. Linear stability analysis on compressible mixing layers by Ragab and Wu [7] show that reducing the Reynolds number reduces the perturbation growth rate at all frequencies. The growth calculated from their analysis for three-dimensional disturbances matched with experimental growth rate at low Mach numbers. Jackson and Grosch [8] have also conducted linear stability analysis of the mixing layer, and showed that beyond a critical Mach number there exist two groups of unstable waves, a fast mode and a slow mode.

In his pioneering work, Chapman [9] shows, using self-similar analysis of laminar compressible mixing layers, that the growth rate for a constant Reynolds number would decrease with increasing M_c. A similar inference is made in turbulent mixing layers as the turbulent kinetic energy production reduces as the M_c increases [10–12]. Karimi and Girimaji [13] showed that spanwise perturbation in the incompressible mixing layers which induces lift-up instability [14] were unaffected by M_c. Streamwise perturbations, however, were shown to stabilize with increase in M_c. The stability of streamwise perturbations at larger Mach number was due to the wavelike nature of pressure, leading to winding and unwinding of roll-up billows [15].

[*]Present address: Department of Aerospace Engineering, Indian Institute of Technology Madras, Chennai-600036, India; ae16d421@smail.iitm.ac.in
[†]sameen@ae.iitm.ac.in
[‡]sbalaji@iitm.ac.in
[§]girimaji@tamu.edu

The degree of rarefaction is parametrized by Knudsen number $\mathrm{Kn} = \lambda/L_\infty$, where λ is the mean-free path, and L_∞ is the characteristic length scale. Most studies on the effect of slight rarefaction in canonical flow instability, such as in Rayleigh-Bénard (RB) [16], Taylor-Couette [17], and Kolmogorov flow [18], have examined the effect of slip at the wall. These studies investigate flow stability using the Navier-Stokes equation with modified boundary conditions due to the slip at the wall. Numerical studies using the direct simulation Monte Carlo approach have also been performed by Stefanov *et al.* [19] and Stefanov and Cercignani [20] on such flows. Ben-Ami and Manela [16] found that the constant heat flux boundary condition is more destabilizing than the constant temperature boundary condition, as it increases the range of Knudsen number at which the flow is unstable. Stefanov *et al.* [19] identified a hysteresis between two attractors of RB flow. Both of the works mentioned above show that at lower Froude number compressibility effects force the convection cells to the vicinity of the colder wall. Manela and Frankel [17] find that the critical Reynolds number, defined in a way that accounts for the variation of temperature changes, remains the same at higher Mach number as well. However, the effect of rarefaction on the KH instability is less understood. The objectives of this paper are to (a) investigate the combined effects of Mach and Knudsen numbers on the stability of two-dimensional mixing layers and (b) characterize the flow physics at various Re-Kn-M_c regimes. Direct numerical simulations of mixing layers for various combinations of M_c and Kn are performed by solving the Bhatnagar-Gross-Krook (BGK) Boltzmann equation.

II. NUMERICAL METHOD AND VALIDATION

The finite-volume-based unified gas kinetic scheme (UGKS) [21] is used to solve the BGK-Boltzmann transport equation [22]:

$$\frac{\partial f}{\partial t} + c_i \frac{\partial f}{\partial x_i} = \nu(f_0 - f), \tag{1}$$

where f is the particle distribution function, c_i is the particle velocity, f_0 is the Maxwellian equilibrium distribution function, and ν is called the collision frequency. The Maxwellian equilibrium distribution f_0 is given as

$$f_0 = \rho\left(\frac{m}{2\pi kT}\right)^{3/2} \exp\left(-\frac{m}{2kT}((c_i - U_i)^2)\right). \tag{2}$$

In the UGKS, the velocity space is also discretized, unlike other continuum solvers. The fluxes are computed using analytical solution of the BGK-Boltzmann equation. The particle distribution functions at the cell interface are obtained using a third-order weighted essentially non-oscillatory reconstruction [23], to study rarefaction effects in cavity flow by Venugopal *et al.* [24]. Ragta *et al.* [25] showed that the three-dimensional (3D) UGKS scheme could accurately capture turbulence at low Reynolds number. The two-dimensional (2D) flow domain, mean flow velocity field, and boundary conditions used in this study are shown in Fig. 1. The parameters which govern the evolution of the mixing layer in addition to M_c, Kn, and Re are Prandtl number (Pr = 1), and the ratio of specific heat capacity ($\gamma = 1.667$). Since monatomic gas

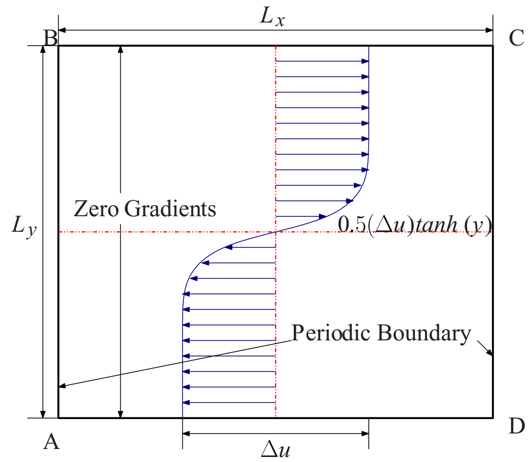

FIG. 1. Computational domain showing the initial averaged velocity profile and boundary conditions.

has been considered, the bulk viscosity is zero. The effects of nonzero bulk viscosity on turbulent compressible flow have been discussed in a few recent investigations [26–28]. According to the work of Boukharfane *et al.* [26], wherein they considered a nonreactive two-species mixing layer for zero and nonzero bulk viscosity in the presence of an oblique shock, the development of turbulent kinetic energy was unaffected by the presence of bulk viscosity. However, it was also shown by Chen *et al.* [27] and Pan *et al.* [28] that for homogeneous turbulence, the flow approaches the incompressible regime as bulk viscosity increases. This can be attributed to the macroscopic effect of bulk viscosity at resisting dilatation. It was shown by Jackson and Grosch [29] that upon changing Prandtl number, the qualitative results obtained for the compressible mixing layer remain unchanged. While this work has been for Pr = 1, the inferences are expected to be qualitatively similar for a different Prandtl number.

Using the hard-sphere model [25], M_c, Re, and Kn are related as

$$\mathrm{Re} = \frac{16}{5}\frac{M_c}{\mathrm{Kn}}\sqrt{\frac{\gamma}{2\pi}}. \tag{3}$$

We examine the effect of M_c and Kn on mixing layers using three indicators, namely, vorticity thickness ($\delta = \Delta u/\omega_{\max}$), momentum thickness [$\delta_m = 1/\rho_\infty \int_{-\infty}^{\infty} \bar{\rho}(1/4 - \tilde{u}_x^2/\Delta u^2)dy$], and volume-averaged perturbation kinetic energy [$k = (1/V)\int_{-\infty}^{\infty} \frac{1}{2}u_i'' u_i'' dV$]. Here, $\omega_{\max} = \max(\partial\tilde{u}_x/\partial y)$ represents the maximum vorticity computed using the Favre-averaged streamwise velocity, $\tilde{u}_x$. The Favre average of a variable q is given as $\tilde{q} = (\overline{\rho q})/(\bar{\rho})$, with the overbar representing Reynolds averaging, and corresponding velocity perturbation is obtained as $u_i'' = u_i - \tilde{u}_i$.

All the variables are nondimensionalized using the freestream temperature T_∞, freestream density ρ_∞, most probable speed $c_\infty = \sqrt{2RT_\infty}$, and initial vorticity thickness δ_0. The mean velocity is given by $\tilde{u}(x, y) = 0.5(\Delta u)\tanh(y)$, which is seeded with harmonic ($k_x\delta_0 = 0.628$, wavelength equal to half the domain length in the streamwise direction) and subharmonic ($k_x\delta_0 = 0.314$, wavelength equal to the domain length in the streamwise direction) solenoidal

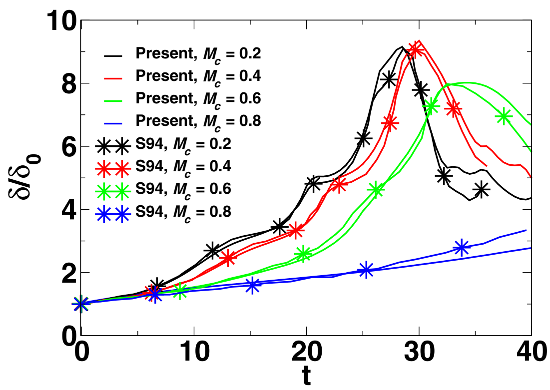

FIG. 2. Comparison of present work against Sandham's [30] result (S94) for $M_c = 0.2$–0.8 and Re = 200.

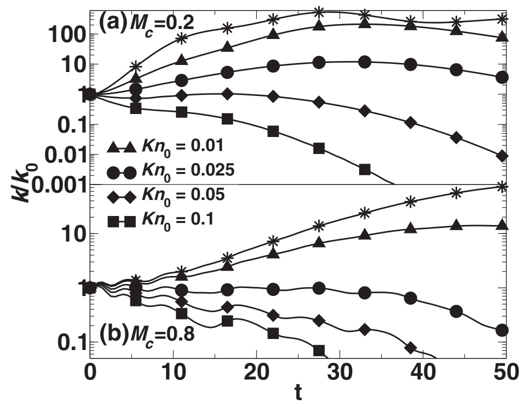

FIG. 3. Development of normalized perturbation kinetic energy at (a) $M_c = 0.2$ and (b) $M_c = 0.8$. The legend symbol (*) is for (a) $\mathrm{Kn}_0 = 1.65 \times 10^{-3}$ and (b) $\mathrm{Kn}_0 = 6.6 \times 10^{-3}$.

perturbations, following Sandham [30]. These perturbations are also close to the minima of the marginal stability curve reported by Bhattacharya *et al.* [3].

The initial temperature distribution follows the Crocco-Busemann relationship and the pressure is kept constant throughout the domain. The initial densities of both the freestreams are equal. The particle distribution function is initialized as a Maxwellian distribution function. The UGKS computation has been validated for Re = 200.0 for various M_c at Kn $\approx 10^{-3}$. The evolution of the vorticity thickness with time (scaled by $2\delta_0/\Delta u$) is compared against the continuum results of Sandham [30] in Fig. 2. A grid independence study has been conducted for all the cases presented in the present problem.

III. RESULTS

Simulations are performed by varying the M_c and initial Knudsen number, Kn_0. As the mixing layer develops, the instantaneous Knudsen number, $\mathrm{Kn}(t) = Kn_0\delta_0/\delta$, changes since the thickness of the mixing layer evolves with time. The Reynolds number correspondingly changes according to Eq. (3). The evolution of mixing layer thickness and perturbation kinetic energy are computed and analyzed.

A. Perturbation kinetic energy

The time evolution of k/k_0 for $M_c = 0.2$ and 0.8 at various Kn_0 are plotted in Fig. 3. Low Kn_0 cases exhibit the canonical instability. For other cases the ultimate k/k_0 decay rate increases with increase in Kn_0. It can also be seen that the decay rate is faster at lower M_c for a given Kn_0. From Eq. (3), at a given Kn, an increase in M_c implies an increase in Re. Thus, the reduced decay rate of k may be due to the increase in Reynolds number, which reduces viscous effects. This is consistent with the findings of Betchkov and Szewczyk [1], that decreasing the Reynolds number reduces the growth rate for an incompressible flow, even though the inception of KH instability is due to an inviscid mechanism.

It is also interesting to note that for $M_c = 0.2$, the k/k_0 time evolution is nonmonotonic for $\mathrm{Kn}_0 < 0.05$ and monotonically decaying for $\mathrm{Kn}_0 > 0.05$. A similar observation can be made from Fig. 3(b) as well, where the flow starts decaying (although not monotonically) for $\mathrm{Kn}_0 > 0.025$. Indeed, the stabilization depends on Re and wavenumber, as shown by Bhattacharya *et al.* [3], and there exists a critical Re below which there is no amplification of perturbation kinetic energy, which depends on M_c and Kn as given in Eq. (3).

In high M_c flows, Karimi *et al.* [15] have demonstrated that due to the dilatational nature of velocity there is a delay in the development of KH instability, as it leads to the rolling and unrolling of the vortex. It is important to note that the effect of increasing Kn_0 is to stabilize the flow irrespective of M_c or compressibility. The nonmonotonic behavior will be examined later.

B. Mixing layer thickness

Next the evolution of mixing layer thickness is examined for various Kn_0 and M_c. Figures 4 and 5 show the development of vorticity thickness and momentum thickness of the mixing layer with time. Ragab and Wu [7] showed using 3D linear stability of the compressible mixing layer that the growth rate decreases with increase in M_c. At small Kn_0, Fig. 4(a) shows that the mixing layer thickness exhibits a nonmonotonic increase with time. The mixing layer thickness

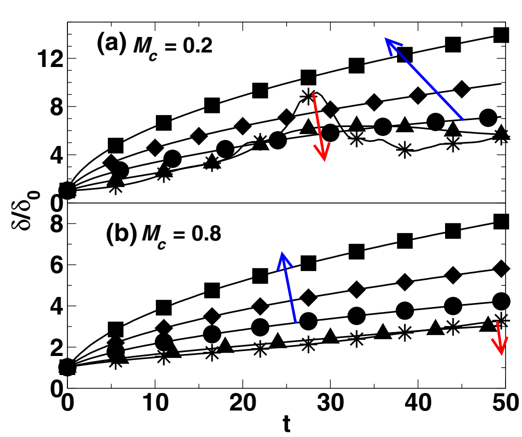

FIG. 4. Development of vorticity thickness. The legend is the same as in Fig. 3.

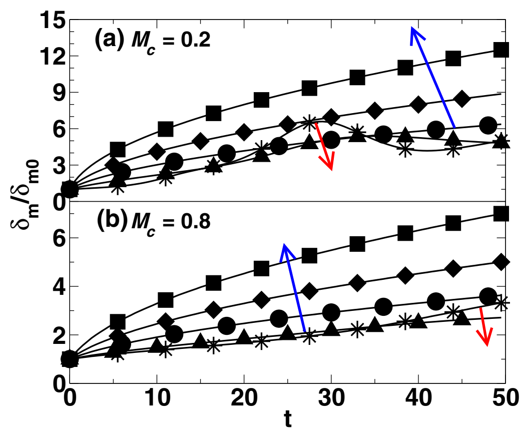

FIG. 5. Development of momentum thickness. The legend is the same as in Fig. 3.

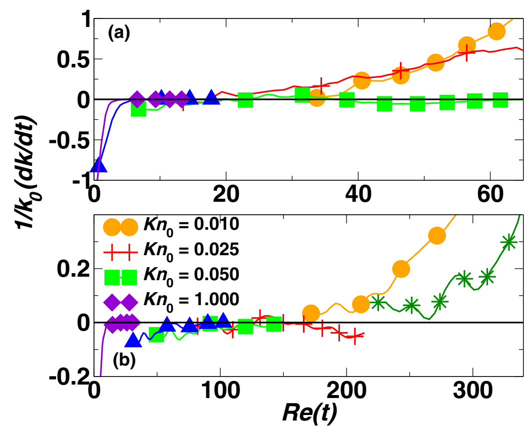

FIG. 6. Evolution of perturbation kinetic energy for various Kn_0 for (a) $M_c = 0.2$, (b) $M_c = 0.8$. The blue triangle is (a) $\mathrm{Kn}_0 = 0.5$ and (b) $\mathrm{Kn}_0 = 0.1$. The green asterisk is (b) $\mathrm{Kn}_0 = 6.59 \times 10^{-3}$.

has an initial exponential growth followed by a decrease. It is seen that at these small Kn_0, the peak mixing layer thickness decreases with increase in Kn_0, in effect implying that the growth rate decreases with increase in Kn_0 [shown by the downward pointing red arrow in Fig. 4(a)]. At larger Kn_0, the growth rate is monotonic, and it increases with increase in Kn_0, which is shown by the upward pointing blue arrow. The nonmonotonic growth in the mixing layer thickness is seen for cases which show amplification in the perturbation kinetic energy, i.e., the unstable cases. Interestingly, the monotonic mixing layer growth is seen for cases which show decay in perturbation kinetic energy, i.e., the stable cases.

For $M_c = 0.8$, it is seen that at high Kn_0 (stable cases), the growth rate is monotonic and increases with increase in Kn_0; however, it is slower in comparison to $M_c = 0.2$. At low Kn_0 (unstable cases) as well, it is seen that the growth rate is slower than $M_c = 0.2$, but, similar to what was seen in $M_c = 0.2$, the growth rate decreases with increase in Kn_0. From Fig. 4 and Fig. 5, both the vorticity thickness and the momentum thickness are of a similar order of magnitude, and they follow similar trends as the mixing layer develops. The conclusions drawn from the vorticity thickness plots are applicable for momentum thickness development as well.

C. Regimes of mixing layer

All the computations above are initiated with a particular Re_0, and Re evolves with time since δ increases with time. The rate of change of k/k_0 against instantaneous Reynolds number, $\mathrm{Re}(t) = \mathrm{Re}_0\delta/\delta_0$, for various Kn_0 is shown in Figs. 6(a) and 6(b) for $M_c = 0.2$ and 0.8, respectively. It is seen that the flow becomes unstable ($dk/dt > 0$) only if $\mathrm{Re}(t) > \mathrm{Re}_{cr}$ at some stage of the evolution. Here, Re_{cr} refers to the Reynolds number at which marginal stability is obtained. The Reynolds number at which the flow starts showing positive dk/dt is noted as Re_{cr} for each convective Mach number. We examine only the initial unsteady development in this paper. The computed values of Re_{cr} obtained for various M_c are tabulated in Table I. For larger M_c, due to the oscillations in the perturbation kinetic energy mentioned in Sec. III A, smoothening needs to be applied to the time derivative and hence the exact value of Re_{cr} cannot be deduced. For the incompressible regime, Re_{cr} is approximately constant; however, in the compressible regime, Re_{cr} increases with increase in M_c. The corresponding Kn_{cr} can be obtained from Eq. (3).

In the earlier discussion, it was shown that the effect of compressibility on the evolution of k/k_0 is nonmonotonic. It was also seen that the Kn has a stabilizing effect. Based on this, five different regimes in the Kn-Re-M_c parameter space are proposed. The flow physics of these regimes will be analyzed in detail in a full paper. The present paper discusses only the important features.

Low-Kn, low-M_c regimes. Figures 7(a)–7(c) show the vorticity contours at three instants, as the mixing layer develops in this regime for the case of $M_c = 0.2$ and $\mathrm{Kn}_0 \approx 10^{-3}$. In this regime, the flow is unstable and exhibits classical KH instability. Since the Mach number is low, the velocity field is solenoidal in nature [15]. The perturbation kinetic energy amplifies without any oscillations. The mixing layer thickness shows a nonmonotonic growth, with the growth rate of the mixing layer thickness decreasing with increase in Knudsen number.

High Kn, low M_c. Figures 7(d)–7(f) show the vorticity contour of the mixing layer in this regime for $M_c = 0.2$ and $\mathrm{Kn}_0 = 0.1$ at different instants. Since $\mathscr{O}(\mathrm{Re}) = 1$, the flow is dominated by viscous effects, and since the Mach number is low, the velocity field is solenoidal in nature. At high enough Knudsen number, ballistic effects of rarefaction occur. Ballistic effect refers to the phenomenon in which collision between molecules becomes less frequent than in continuum cases [24]. This has two consequences: increased mean-free path and increased effective viscosity. The increased effective viscosity leads to a monotonic decay in the perturbation kinetic energy. On the other hand, the increase in the mean-free

TABLE I. Variation of critical Reynolds number with M_c.

M_c	0.1–0.4	0.5	0.6	0.7	0.8	0.9	1.0
Re_{cr}	20	35–40	45–50	70–80	120–150	190–200	300–350

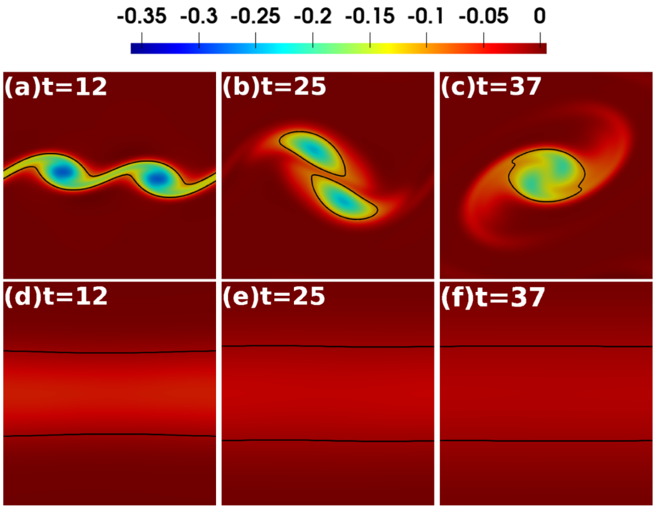

FIG. 7. Contour of vorticity for $M_c = 0.2$ and (a–c) $\mathrm{Kn}_0 = 1.65 \times 10^{-3}$ and (d–f) $\mathrm{Kn} = 0.1$. The black contour line is for $\omega = -0.1$ (top) and 0.02 (bottom).

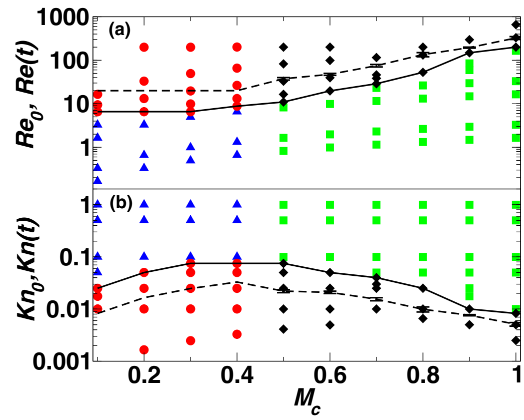

FIG. 9. Map indicating low Kn and low M_c (red circles), low Kn and intermediate M_c (black diamond), high Kn and low M_c (blue triangle), and high Kn and high M_c (green square) regimes in (a) M_c-Re space and (b) Kn-Re space.

path causes the momentum and vorticity thickness to grow. It can be seen in the figure that the vorticity merely diffuses away without the formation of roll-ups. In this regime, the mixing layer thickness growth rate is extremely high and increases with increase in Knudsen number.

Low Kn, intermediate M_c. Figures 8(a)–8(c) show the vorticity contour in this regime for the case of $M_c = 0.8$ and $\mathrm{Kn}_0 \approx 10^{-3}$. This regime also exhibits KH instability. The Reynolds number is higher than the Re_{cr}, implying that the flow is unstable. Since the Mach number is higher, both dilatational (delay in vortex formation due to the wavelike nature of pressure) and solenoidal (formation of vortex roll-up billow) effects are seen, consistent with [15]. It is seen that the vortex roll-up is delayed, and the vortices are stretched, as compared to $M_c = 0.2$ at low Kn_0. It is seen that only one roll-up billow is formed instead of two seen in Fig. 7. The perturbation kinetic energy increases with time, although this growth is delayed. The growth rate of the mixing layer thickness at this regime is much slower than the lower Mach number regime.

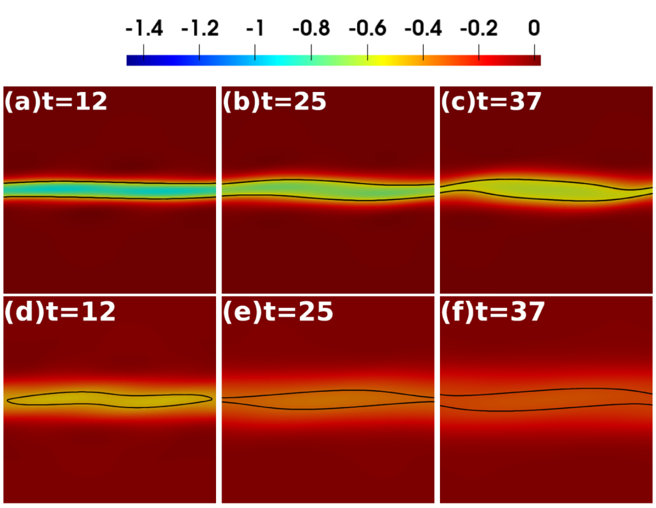

FIG. 8. Contour of vorticity for $M_c = 0.8$ and (a–c) $\mathrm{Kn}_0 = 8.24 \times 10^{-3}$ and (d–f) $\mathrm{Kn}_0 = 0.05$. The black contour line is for $\omega = -0.5$ (top) and $-0.9 \times \omega_{\mathrm{peak}}$ (bottom).

Low Kn, high M_c. In these cases, $\mathscr{O}(\mathrm{Re}) \geqslant 10$, implying advective terms dominate the evolution of the mixing layer. The velocity field is largely dilatational. These cases correspond to $M_c > 1$, for which the figures are not included for the sake of brevity. The vortices wind and unwind about the pivot point, and the KH instability does not manifest [15]. In this regime, there is no amplification in perturbation kinetic energy. The growth rate of the mixing layer thickness is extremely slow as viscous effects are minimal.

High Kn, high M_c. Figures 8(d)–8(f) show vorticity contours for $M_c = 0.8$ and $\mathrm{Kn}_0 = 0.05$ as a sample case for this regime, seen at high Knudsen number and convective Mach number. In Figs. 8(d)–8(f), the vorticity contour lines are chosen closer to the center of the mixing layer, and it clearly shows that the mixing layer rolls, unrolls, and diffuses as it develops. Due to the higher Knudsen number, viscous effects are considerable. In this regime, the perturbation kinetic energy shows an oscillatory behavior; however, it does not amplify as the mixing layer develops [see the blue triangle curve in Fig. 6(b)]. Due to viscous and ballistic effects, the mixing layer thickness growth rate is high.

Based on the above discussions, we identify different regimes of physics on the M_c-Kn-Re parameter space. The map in Fig. 9 is made by grouping the different regimes mentioned above. From Fig. 9, the demarcations of these regimes are evident. In Fig. 9(a), the solid black line demarcates values of Re_0, above which simulations are unstable and below which simulations are stable.

Similarly, in Fig. 9(b), the simulations with Kn_0 below the solid black line are unstable, and above are stable. The dashed black line gives the value (or range of values) of Re_{cr} and Kn_{cr}. Figures 9(a) shows that in the incompressible regime, the flow has $\mathrm{Re}_{cr} = 20$, suggesting that at low M_c, the only parameter affecting stability is Re. For the compressible regime, as the Mach number increases, the Re_{cr} also increases. In Fig. 9(b), it is seen that Kn_{cr} increases linearly with M_c for incompressible cases and decreases for compressible cases.

IV. CONCLUSION

Rarefaction profoundly affects the stability of two-dimensional mixing layers. In the continuum incompressible regime, these flows exhibit the classical Kelvin-Helmholtz instability. A series of simulations is performed using the UGKS methodology over a wide range of Mach and Knudsen numbers to investigate rarefaction effects on the KH instability and contrast them against compressibility effects.

The major contributions of the present work are discussed below. Five distinct stability regimes in the Reynolds-Mach-Knudsen number parameter space are demarcated. The first is the low M_c, low Kn KH regime in which vortices roll up about the pivot point, leading to the onset of the instability. Along with the perturbation kinetic energy, the vorticity and momentum thicknesses of the mixing layer grow exponentially in the linear regime of evolution. The critical Reynolds number, in this case, is about 20, which is within the range established in the literature. The next regime identified is the intermediate M_c, low Kn range. While the flow continues to be unstable in this regime, the advent of dilatational fluctuations renders the nature of the flow field distinctly different from the purely incompressible regime. The instability growth rate is distinctly slower than the incompressible regime, and the critical Reynolds number increases with Mach number. The third regime occurs in the high M_c range. In this case, the wavelike dilatational fluctuations dominate. The growth of kinetic energy and vorticity and momentum thicknesses are completely suppressed. The final two regimes are characterized by high Kn. In these regimes, viscous-diffusive action brought about by ballistic transport is most dominant. This leads to two important outcomes: the suppression of perturbation kinetic energy and diffusive growth of vorticity and momentum thicknesses. These regimes are classified as stable due to the suppression of perturbation kinetic energy, although the momentum and vorticity thicknesses grow.

ACKNOWLEDGMENTS

We acknowledge the use of the computing resources at HPCE, IIT Madras. The authors thank SPARC from the government of India for funding this project.

[1] R. Betchov and A. Szewczyk, Stability of a shear layer between parallel streams, Phys. Fluids **6**, 1391 (1963).
[2] E. Villermaux, On the role of viscosity in shear instabilities, Phys. Fluids **10**, 368 (1998).
[3] P. Bhattacharya, M. P. Manoharan, R. Godindarajan, and R. Narasimha, The critical Reynolds number of a laminar incompressible mixing layer from minimal composite theory, J. Fluid Mech. **565**, 105 (2006).
[4] D. Papamoschou and A. Roshko, The compressible turbulent shear layer: An experimental study, J. Fluid Mech. **197**, 453 (1988).
[5] M. Lessen, J. A. Fox, and H. M. Zien, On the inviscid stability of the laminar mixing of two parallel streams of a compressible fluid, J. Fluid Mech. **23**, 355 (1965).
[6] N. D. Sandham and W. C. Reynolds, Compressible mixing layer -linear theory and direct simulation, AIAA J. **28**, 618 (1990).
[7] S. A. Ragab and J. L. Wu, Linear instabilities in two-dimensional compressible mixing layers, Phys. Fluids A **1**, 957 (1989).
[8] T. L. Jackson and C. E. Grosch, Inviscid spatial stability of a compressible mixing layer, J. Fluid Mech. **208**, 609 (1989).
[9] D. R. Chapman, Laminar mixing in compressible fluids, NACA Technical Notes, NACA-TN-1800 (1949).
[10] A. W. Vreman, N. D. Sandham, and K. H. Luo, Compressible mixing layer growth rate and turbulence characteristics, J. Fluid Mech. **320**, 235 (1996).
[11] C. Pantano and S. Sarkar, A study of compressibility effects in the high-speed turbulent shear layer using direct simulation, J. Fluid Mech. **451**, 329 (2002).
[12] S. Arun, A. Sameen, B. Srinivasan, and S. S. Girimaji, Topology-based characterization of compressibility effects in mixing layers, J. Fluid Mech. **874**, 38 (2019).
[13] M. Karimi and S. S. Girimaji, Influence of orientation on the evolution of small perturbations in compressible shear layers with inflection points, Phys. Rev. E **95**, 033112 (2017).
[14] C. Arratia, C. P. Caulfield, and J.-M. Chomaz, Transient perturbation growth in time-dependent mixing layers, J. Fluid Mech. **717**, 90 (2013).
[15] M. Karimi and S. S. Girimaji, Suppression mechanism of Kelvin-Helmholtz instability in compressible fluid flows, Phys. Rev. E **93**, 041102(R) (2016).
[16] Y. Ben-Ami and A. Manela, Effect of heat-flux boundary conditions on the Rayleigh-Bénard instability in a rarefied gas, Phys. Rev. Fluids **4**, 033402 (2019).
[17] A. Manela and I. Frankel, On the compressible Taylor-Couette problem, J. Fluid Mech. **588**, 59 (2007).
[18] A. Manela and J. Zhang, The effect of compressibility on the stability of wall-bounded Kolmogorov flow, J. Fluid Mech. **694**, 29 (2012).
[19] S. Stefanov, V. Roussinov, and C. Cercignani, Rayleigh-Bénard flow of a rarefied gas and its attractors. I. Convection regime, Phys. Fluids **14**, 2255 (2002).
[20] S. Stefanov and C. Cercignani, Monte Carlo simulation of the Taylor-Couette flow of a rarefied gas, J. Fluid Mech. **256**, 199 (1993).
[21] J.-C. Huang, K. Xu, and P. Yu, A unified gas-kinetic scheme for continuum and rarefied flows II: Multi-dimensional cases, Commun. Comput. Phys. **12**, 662 (2012).
[22] P. L. Bhatnagar, E. P. Gross, and M. Krook, A model for collision processes in gases. I. Small amplitude processes in charged and neutral one-component systems, Phys. Rev. **94**, 511 (1954).
[23] V. Venugopal and S. S. Girimaji, Unified gas kinetic scheme and direct simulation Monte Carlo computations of high-speed lid-driven microcavity flows, Commun. Comput. Phys. **17**, 1127 (2015).
[24] V. Venugopal, D. S. Praturi, and S. S. Girimaji, Non-equilibrium thermal transport and entropy analyses in rarefied cavity flows, J. Fluid Mech. **864**, 995 (2019).

[25] L. K. Ragta, B. Srinivasan, and S. S. Sinha, Efficient simulation of multidimensional continuum and non-continuum flows by a parallelised unified gas kinetic scheme solver, Int. J. Comput. Fluid Dyn. **31**, 292 (2017).
[26] R. Boukharfane, P. J. M. Ferrer, A. Mura, and V. Giovangigli, On the role of bulk viscosity in compressible reactive shear layer developments, Eur. J. Mech. B Fluids **77**, 32 (2019).
[27] S. Chen, X. Wang, J. Wang, M. Wan, H. Li, and S. Chen, Effects of bulk viscosity on compressible homogeneous turbulence, Phys. Fluids **31**, 085115 (2019).
[28] S. Pan and E. Johnsen, The role of bulk viscosity on the decay of compressible, homogeneous, isotropic turbulence, J. Fluid Mech. **833**, 717 (2017).
[29] T. L. Jackson and C. E. Grosch, Inviscid spatial stability of a compressible mixing layer. Part 3. Effect of thermodynamics, J. Fluid Mech. **224**, 159 (1991).
[30] N. D. Sandham, The effect of compressibility on vortex pairing, Phys. Fluids **6**, 1063 (1994).

Correction: The omission of a support statement in the Acknowledgments has been fixed.